Article title:

The COOLER code: a novel analytical approach to calculate sub-cellular energy deposition by internal electron emitters.

Author names:

Mattia Siragusa[1,*], Giorgio Baiocco[2], Pil M. Fredericia[1,*], Werner Friedland[3], Torsten Groesser[1], Andrea Ottolenghi[2], Mikael Jensen[1]; *Scholar In Training

Affiliations:

[1]Hevesy Laboratory, Center for Nuclear Technologies, Technical University of Denmark, Denmark.

[2]Department of Physics, University of Pavia, Pavia, Italy.

3Institute of Radiation Protection, Helmholtz Zentrum München – German Research Center for Environmental Health, Neuherberg, Germany.

Proposed running title:

Energy deposition by internal electron emitters

Corresponding author:

Mattia Siragusa

Corresponding author contact information:

Mattia Siragusa, Hevesy Laboratory, Technical University of Denmark, Center for Nuclear Technologies, Risø Campus, Frederiksborgvej 399, 4000 Roskilde, Denmark. E-mail: masir@dtu.dk

Mattia Siragusa, Giorgio Baiocco, Pil M. Fredericia, Werner Friedland, Torsten Groesser, Andrea Ottolenghi, Mikael Jensen. The COOLER code: a novel analytical approach to calculate sub-cellular energy deposition by internal electron emitters.

ABSTRACT:

Absorbed dose calculations in nuclear medicine are conventionally based on the formalism introduced by the Medical Internal Radiation Dose (MIRD) committee. The so called S-value, that is, the dose to a target region per decay in a source region, represents the primary quantity in the formalism. When extending the formalism to the cellular level and to low energy electron emitters, MIRD uses Geometric Reduction Factors (GRF) and Cole's "effective" stopping power, derived from electron transmission experiments in air and plastic foils. In this work, S-values are determined through a new analytical approach relying on the convolution of two main terms: one related to the position of electron sources (the sites of radioactive decays), the other to the density of deposited energy as a function of radial distance from the source. This second term was obtained through full Monte Carlo simulations of electron tracks in liquid water with the code PARTRAC. The proposed method is suitable for Auger-cascade electrons, but can be naturally extended to any energy of interest and to beta spectra. Calculations relying on this new method are entirely entrusted to a dedicated MATLAB-based program code called COOLER (COmputation Of Local Electron Release). Two realistic geometrical models for V79 cells were implemented, for different cell culture conditions (adherent and floating cells).

Results for cellular S-values obtained with COOLER are here validated by full Monte Carlo simulations and compared to MIRD predictions. Electron ranges and energy deposition data as a function of distance from the source are also obtained and discussed. The largest discrepancies between COOLER results and MIRD predictions are generally found for electrons at around 25 keV, where the disagreement in S-values can be higher than 60%. In the calculations for V79 adherent cells, uncertainties in positioning the cell nucleus led to discrepancies in the S-values up to 15%. A comparison between the use of tritium full beta-

decay spectrum and its mean energy to calculate nuclear S-values for a uniform source distribution in the cell is also presented.

The COOLER code will be made available for download from DTU-Nutech website: http://www.nutech.dtu.dk/.

INTRODUCTION

The absorbed dose is usually regarded as the primary quantity for assessment and prediction of the effects induced by ionizing radiation. The aim of any radiation therapy is to deliver a high and lethal dose to malignant cells, while sparing the healthy ones. The need for accurate and precise dose planning and dosimetry is universally accepted in external radiotherapy. It is also normally agreed that internal radiotherapy should aim at delivering predictable and defined radiation doses to tumor targets, and reliable estimates of the collateral radiation dose to non-target organs and tissues have to be made available. In the framework of the International Commission on Radiological Protection (ICRP) and through the work of the Medical Internal Radiation Dose (MIRD) committee, this is today possible with an acceptable precision when using organ S-values, that are defined as the dose to a target region per decay in a source region (*1*), based on the reference man assumptions and using measured or extrapolated organ time-activity curves.

MIRD formalism breaks down completely if the isotopes in question are selected to give highly localized doses, with typical particle ranges equal to or less than one cell diameter. Here, the intracellular activity distribution becomes important, as well as a sub-cellular definition of source and target regions. This is taken into account in the definition of cellular S-values, that have been established by the MIRD committee (*1*). Equally important is the capability to calculate cellular S-values for many other cellular geometries than the simple spherical concentric model used by MIRD.

A robust and generally applicable tool for cellular S-value calculations is of fundamental importance for selection of tracer vectors and radionuclides, for the interpretation of preclinical results, and for the general establishment of doses in any use, therapeutic or diagnostic, of isotopes with significant short range particle emissions.

The generally applicable method of Monte Carlo simulations is normally beyond the practical reach of the preclinical and clinical researcher. In this work an alternative way to obtain cellular S-values is

established, valid in all cases and based on first principles of dose distribution calculations, taking as input only the cell geometry and the emitted particle spectrum of the isotope of interest.

THE ORIGINAL MIRD S-VALUE FORMALISM

The original cellular MIRD formalism relies on the assumption of a uniform activity distribution, with radionuclide sources spread in one or more cellular compartments such as the cell nucleus, the cytoplasm or the whole cell (*1*–*3*). However, radiolabeled molecules able to selectively target tumor cells mostly lead to non-uniform activity distributions (*4*–*8*). A way to counterbalance the effects of tumor cell heterogeneity and poor penetration capabilities of radionuclide carriers was found in the use of penetrating beta emitters (*9,10*). Nonetheless, energy deposition of long-range beta electrons affects healthy cells located in the proximity of the target. Primary Auger-electron emitters are often indicated as better candidates in highly targeted radionuclide therapies (*11*–*14*). Auger electrons are typical products of the results of radionuclides that decay by electron capture or have substantial internal conversion (*15*). Auger events originating from inner-shell vacancies lead to a cascade of successive transitions with several low-energy and short-range electrons (*16*), here all conveniently called Auger electrons.

The starting point to derive MIRD formalism for mono-energetic electrons consists in expressing the absorbed dose D (Gy) as:

$$D = \frac{wA\sum_i n_i E_i \phi_i}{m}, \qquad (1)$$

where D is the absorbed dose and A is the cumulated activity (Bq·s), n_i is the number of particles with energy E_i (keV) emitted per nuclear transition. ϕ_i is the absorbed fraction, *i.e.* the fraction of energy emitted from the source region that is absorbed in the target region for the *i*-th radiation component, m is the mass of the target region (kg) and w is a constant to express D in Gy. The original MIRD formalism

consists in a general method to convert administered activity into specific organ radiation dose. S-values are defined through the following expression, giving the absorbed dose in the target region D_{rk}:

$$D_{r_k} = \sum_h A_h S(r_k \leftarrow r_h), \qquad (2)$$

where r_k and r_h are the target and the source region respectively and A_h is the cumulated activity in the source region. This can be easily generalized to the cellular level, with cellular sub-compartments as targets and source regions. The decay of radionuclides normally have more than one electron branch and many Auger-cascade electrons, each with a well-defined energy E_i, associated to a certain probability of emission. S can be calculated for a fixed combination of source and target regions replacing D in Eq. (2) with its expression given in Eq. (1), so that:

$$S(r_k \leftarrow r_h) = \frac{w \sum_i n_i E_i \phi_i(r_k \leftarrow r_h)}{m_{r_k}}. \qquad (3)$$

To find individual terms in Eq. (3), MIRD calculates Geometric Reduction Factors (GRFs). GRFs provide the efficacy of irradiation at a certain distance from the source point in terms of the fraction of the sphere centered on the emission point that overlaps with the target volume (*1*). The absorbed fraction ϕ_i is then written as the following convolution integral:

$$\phi_i(r_k \leftarrow r_h) = \frac{1}{E_i} \int_0^\infty \Psi_{r_k \leftarrow r_h}(x) \cdot \frac{dE}{dX}\Big|_{X(E_i)-x} dx, \qquad (4)$$

where $\Psi_{r_k \leftarrow r_h}(x)$ is the GRF and $\frac{dE}{dX}\Big|_{X(E_i)-x}$ is the stopping power evaluated at $X(E_i) - x$, *i.e.* the residual range of a particle with initial energy E_i after a distance (linear distance *(17)*) x through the medium. For electrons with energies ranging from 20 eV to 20 MeV, MIRD adopts Cole's formulas (minor changes introduced by Howell et al. (*18*) are not discussed here):

$$\begin{cases} E(X) = 5.9(X + 0.007)^{0.565} + 0.00413X^{1.33} - 0.367 \\ \dfrac{dE}{dX}(E) = 3.316(X + 0.007)^{-0.435} + 0.0055X^{0.33} \end{cases}, \qquad (5)$$

where X is the particle range, defined as the thickness of an absorber stopping 95% of incident particles (*i.e.* at a 5% transmission level). The units in Eq.s (5) are: E in keV, X in 100 μg/cm^2 (or μm at unit density) and dE/dX in keV·cm^2 per 100 μg (equivalent to keV/μm at unit density). Cole's stopping power has the units of a stopping power, and it is obtained as the derivative of the energy versus range dependence measured in electron transmission experiments in air and plastic foils (*19*). In this sense it could be referred as an "effective" stopping power (17). Beside the adoption of Cole's formula, the convolution integral method adopted by MIRD has some well-known limitations. As the calculation of GRFs is not trivial, cellular S-values can be defined only for simple geometries. In addition to that, the adoption of the Continuous Slowing Down Approximation (CSDA) - implicit in Eq. (4) - neglects by construction the finite range of delta rays as well as angular deflections and straggling effects which are relevant at the subcellular level (*2,20*). The CSDA approach might be questioned as the energy straggling, angular deflections and δ -rays cannot be neglected at the subcellular scale (*17,21*).

A NEW ANALYTICAL APPROACH TO CALCULATE S-VALUES

The analytical method proposed in this work avoids the limitations coming from the use of GRFs to calculate S-values. Instead, in the calculations quantities containing information on the spatial distribution of electron emitters are used, namely the sites of radioactive decay where the primary electron track originates. Moreover, the proposed method replaces the use of Cole's effective stopping power by the adoption of energy deposition data tables derived from full Monte Carlo simulations of electron track structure with the biophysical code PARTRAC (the use of any convenient analytical expressions of energy deposition versus distance is also possible). In the proposed approach energy-dependent terms are completely separated from the geometrical terms. The method relies on the convolution of two main terms: one related to the position of electron sources in different cellular compartments, the other to the

density of deposited energy in water as a function of distance from the source. Electron energies were chosen between 5 and 50 keV. The proposed method can be naturally extended to any energy of interest, with the possibility of being optimized for Auger-emitter radiotherapy. Starting from first principles, our tool surpasses most of the problems coming with the original MIRD method. It is based on an analytical approach, and presented results are validated with full track structure Monte Carlo calculations with the code PARTRAC. Calculations relying on this new method are entirely entrusted to a dedicated MATLAB-based (*22*) program code called COOLER (COmputation Of Local Electron Release). Description of the code and its validation are discussed in detail in this work. Electron ranges and energy deposition data as a function of distance from the source are also obtained and discussed. Results for electron S-values as a function of energy are presented for different activity distribution scenarios and compared to MIRD predictions. The method can be generalized for continuous spectra, for example the tritium spectrum.

MATERIALS AND METHODS

THE PARTRAC CODE

Monte Carlo track-structure codes that simulate the electron slowing down process in an event by event manner can accurately describe the discrete nature of physical interactions, overcoming most of the deficiencies of the MIRD approach (*23*). As a detailed simulation of electron tracks can be time consuming, condensed-history transport codes have often been employed to approach various cellular dosimetric problems (*24–30*). Among the shortcomings of using condensed-history codes, we point out the adoption of large energy cut-off for electron transport, typically between 1 and 10 keV, which results in a spatial resolution of the order of the biological target.

In this work, electron track structure calculations for monoenergetic electrons emitted from point sources were carried out using the event by event Monte Carlo code PARTRAC (PARticle TRACks) (*31*). PARTRAC quantitatively follows elementary processes happening during the passage of ionizing radiation through the target. Currently, PARTRAC can simulate photons, electrons, protons, alpha particles and ion tracks in liquid water. For our purposes, it can be employed for electrons from 10 eV to 10 MeV (*31*). Therefore, it appears as a natural choice for examining low energy electrons. Interaction cross sections in liquid water for excitation levels and ionization shells are obtained within the Plane Wave Born Approximation theory with a model for the dielectric function of liquid water. For energies above 10 keV, the relativistic Bethe approximation is used, while a semi-empirical correction factor handles non-Born effects for electrons below 500 eV (*32–34*). Electrons with energies below 10 eV are no longer traced and the residual energy is deposited locally.

In the experimental setup adopted by Cole to derive the effective stopping power expression adopted in the MIRD formalism for cellular S-Values, electrons in the beam are fired along a chosen single direction. *Per contra*, internal electron sources can be thought as isotropic emitters. The two configurations can be simulated in PARTRAC: examples are shown in Fig. 1.

In this work PARTRAC was used for two purposes:

1. Energy deposition simulated data for monoenergetic electrons were obtained and successively implemented for use in COOLER. To this aim, PARTRAC was used to generate 10000 electron tracks emitted isotropically from a point source with energies from 5 to 50 keV. Electron interactions were simulated in an $8 \cdot 10^6$ μm^3 water cube. To avoid the influence of statistical outliers of observed electron ranges, we dismissed from the simulations the 100 tracks depositing energy at the greatest distance from the point source (hence 99% of the tracks were considered). In this sense, the electron range is defined as the radial distance between the point source and the farthest interaction, after removing the 1% longest tracks. Electron range calculations obtained with this procedure are included in the results presented in this work. An analytical fit to electron energy deposition as a function of radial distance has been also derived from PARTRAC data.

2. Calculations of average energy deposition in the cellular nucleus per decay, *i.e.* following the emission of a single electron, for different uniform activity distributions (in the nucleus or in the whole cell) were performed, by implementing in PARTRAC selected cell geometries as detailed in the following. Such calculations were used to check the correct implementation of PARTRAC energy deposition simulated data in COOLER and in more general to validate COOLER results.

THE COOLER CODE

COOLER is written as a suite of MATLAB-based functions (*22*) to calculate local energy deposition, dose and S-values at the sub-cellular level for electrons in liquid water with energies from 5 to 50 keV.

The theoretical approach adopted relies on the following convolution:

$$E_{dep}(\rho) = (A_N * k_{density})(\rho) = \int A_N(\rho') \cdot k_{density}(\rho - \rho') dV', \qquad (6)$$

where E_{dep} is the energy deposited within the target volume (expressed in keV/decay), A_N is the cumulated activity normalized to the total number of decays (1 decay in total) and $k_{density}$ is a function representing the density of deposited energy at the radial coordinate ρ' from the electron emitting source. Such method can be extended to any energy of interest and, in principle, to all charged particles and all cellular geometries.

In the three-dimensional discrete form used for the software implementation A_N and $k_{density}$ are given by two three-dimensional matrices: the activity matrix describes the spatial distribution of the sites of decay in the source region, while the density matrix defines a density of deposited energy in liquid water (keV/ μm^3). This second matrix originates from the interrelation between deposited energy and distance, which reflects the concept of stopping power. Such interrelation is obtained through calculations with the PARTRAC track structure code (*31*,*34*). Calculations associated to Eq. (6) are entrusted to MATLAB-based scripts.

COOLER allows to calculate the amount of energy delivered from well-defined source regions to various target regions, for instance, the cell nucleus or the entire cell. Currently, in terms of source and target regions, COOLER can handle cubes, spheres, ellipsoids and quasi-ellipsoids (ellipsoids laying on a flat surface, with a portion of their volume cut away, to mimic adherent cell culture conditions as detailed in the following) . S-values are calculated converting E_{dep} from keV/decay to Gy/decay using information on the volume and density of the target region, which is typically the nucleus.

The software will be made available for download from DTU-Nutech website: http://www.nutech.dtu.dk/.

ACTIVITY MATRIX

An entire module of COOLER is devoted to handle the distribution of the decay sites in the source region (activity matrix). Currently, this module can handle point, cubical, spherical, ellipsoidal and quasi-ellipsoidal regions, in which electron emitters are uniformly distributed. Among possible geometries for the source region, of major interest are those matching the shapes of possible cellular compartments (*e.g.* the nuclear or the whole cellular volume. Since S-values are expressed in Gy per decay (or, equivalently, Gy Bq^{-1} s^{-1}), the total energy contained in the source region is normalized to the energy of a single electron, *i.e.* to one single decay. Multiplying the S-value by the total number of radioactive decays occurring within the exposure time, we obtain the total dose in Gy imparted to the selected target.

ELECTRON DEPOSITION DATA AND DENSITY MATRIX

Data on spatial energy deposition by electrons obtained from PARTRAC simulations are implemented for use in COOLER for the calculation of density matrices.

Energy density functions are obtained as follows: reprocessing PARTRAC results, we scored the amount of energy delivered within consecutive spherical shells, concentric with the point source. The amount of energy deposited in each shell is then divided by 10000, giving the average result for a single electron track, and then normalized to the volume of each shell, thus obtaining the density function $k_{density}$, which is the density of deposited energy, per track, as a function of the radial distance from the electron emitter. The number of shells is fixed to 300, regardless of the initial electron energy. For electrons between 5 and 50 keV, this value provides accurate density functions in reasonable computing times. Indeed, the accuracy decreases with increasing energy: the higher the energy, the longer the range and the distance between two consecutive sites of scoring (*e.g.* approximately 3 nm at 5 keV and 130 nm at 50 keV).

The density matrix is then built turning $k_{density}$ into a three-dimensional matrix. A collection of density functions was compiled and included into COOLER for electrons with energies ranging from 5 to 50 keV.

The convolution process relies on the rescaling of physical dimensions into their corresponding virtual lengths, expressed in number of cubical voxels. This feature allows to work at different precision levels, where less precision translates into shorter computation times. The scoring of the energy deposition is carried out on the basis of the geometry of the source and the target regions. S-values are calculated multiplying energy deposited in the target region in keV by the conversion factor $1.602 \cdot 10^{-16}$ (J/keV) and dividing by the volume of the target region in μm^3 (typically the nucleus) times the density of water in $kg/\mu m^3$.

CELLULAR GEOMETRIES

COOLER includes as examples two cell models, ideally representing V79 fibroblasts in different culture conditions. We adopted a spherical geometry for free-floating (cells in suspension in the culture medium) V79 cells, modelling the single cell and its nucleus as concentric spheres of unit density (Fig. 2A). The cellular and the nuclear radii were assumed to be 7.1 and 5.2 μm, respectively. However, as cells are often grown as monolayers on plastic surfaces (*e.g.* mylar), we also implemented the configuration of Fig. 2B, in which the nucleus shows an ellipsoidal shape and the cell is modelled as a quasi-ellipsoid, with the cytoplasm being deformed by attachment to the mylar layer. In this second configuration, the cell and its nucleus appear as concentric disks when seen from above. According to experimental observations (*35–38*), geometrical characteristics for the attached cells were assumed to be as follows: the nuclear thickness, the cytoplasm thickness below the nucleus (between the mylar layer and the nucleus) and the projection of the nuclear area on the mylar layer were set as 6.6 μm, 1.4 μm and 134 μm^2 respectively. The thickness of the cytoplasm above the nucleus was set to 175 nm. The dependence of energy deposition results on the exact positioning of the nucleus inside the cell in the adherent cell culture condition was also investigated, as detailed later. Cellular and nuclear volumes were assumed to stay constant in the two configurations, with a cell volume approximately equal to 1500 μm^3. All values are affected by small fluctuations (generally less than 7%), depending on the geometry and the precision level set by the user when the cell model geometry is built.

SOURCE DEFINITION: THE ^{3}H CASE

Besides monoenergetic electrons, COOLER can be run for sources with their own decay spectrum, thus *e.g.* simulating the realistic case of a cellular contamination with a beta-emitting radionuclide. Tritium data for the beta decay spectrum were taken from the freely available software Radiological Toolbox v.3.0.0 (*39*), which contains nuclear decay data assembled in ICRP Publication 107 (*40*). Along with spectral information, the toolbox reports a mean energy value of 5.68 keV and an end-point energy of 18.59 keV.

Tritium (^{3}H), which is radioactive, is found in nature, but can also be produced by man-made processes (*41*). As it decays, it emits a β^- particle whose range is usually less than the typical diameter of a cell (*42*). In this work, we computed a comparison between the use of tritium beta-decay spectrum and its mean energy only to calculate S-values in the case where the radioactivity is uniformly distributed into the whole cell, while the target region consists in the cellular nucleus. For instance, this might be the case of cells exposed to tritiated water that is a radioactive form of water, where ^{1}H atoms are replaced with ^{3}H. As tritiated water behaves just as water, it can freely diffuse in all cellular compartments, satisfying the condition of uniformity.

Table 1: Tritium beta spectrum, normalized and binned for sampling in Monte Carlo calculations

E_1 (keV)	E_2 (keV)	$P(E_1,E_2)$
0	1.86	0.176
1.86	3.72	0.19
3.72	5.58	0.176
5.58	7.44	0.15
7.44	9.3	0.119
9.3	11.15	0.087
11.15	13.01	0.056

13.01	14.87	0.031
14.87	16.73	0.012
16.73	18.59	0.002

Notes. Bins are uniformly distributed in energy, while the total probability of decay is normalized to one. $P(E_1, E_2)$ is the probability of emission of a beta particle with energy between E_1 and E_2.

REFERENCE DATA

THE MIRDcell V2.0.15 TOOL

Rutgers University in collaboration with the MIRD committee developed the Java applet called MIRDcell, whose current version is MIRDcell V2.0.15. It can be accessed from http://www.*mirdcell.njms.rutgers.edu*. The main intent of the software is to provide a user-friendly interface to calculate, for different activity distributions, the S-values and the fractions of cells that survive the exposure to ionizing radiation on the basis of the calculated absorbed doses to the individual cells (*43*). In this work, MIRDcell was employed to obtain S-values in the cellular nucleus for different uniform activity distributions. MIRDcell calculations were used to compare COOLER results with predictions consistent with the MIRD standard. The notation adopted in the software is consistent with that of this paper and with MIRD pamphlet no. 21 (*44*). In MIRDcell monoenergetic electrons with 100% probability of emission were selected to deliver radiation dose to single cells. MIRDcell was run with a cellular geometry similar to that implemented for V79 floating cells, *i.e.* the cell and its nucleus were modelled as 2 concentric spheres with radii of 7 and 5 μm, respectively (the choice of the numerical values was limited by the applet running only with integer numbers). As in COOLER, cells were assumed to be composed of liquid water of unit density. The radioactivity was assumed to be uniformly distributed in the source region, selected among the cell nucleus (N) and the cytoplasm (Cy). The target region for absorbed dose calculations was the cell nucleus. As in the MIRD monograph (*1*), the effective stopping power relationship of Cole was used for electrons. Since MIRDcell does not directly include the N←Cell

case, this was calculated by means of the volumes V_N and V_{Cy} of the different cellular compartments as in the following equation:

$$S_{N\leftarrow Cell} = \frac{S_{N\leftarrow N}V_N + S_{N\leftarrow Cy}V_{Cy}}{V_{Cell}}. \qquad (7)$$

THE NIST-ESTAR DATABASE

The NIST-ESTAR database (45) provides stopping power and range values for electrons in different materials, including liquid water. Data are expressed as a function of energy and given for electrons between 10 keV and 1 GeV. Collision stopping powers are estimated from Bethe's theory (46,47) and density effect corrections are calculated as explained by Sternheimer (48,49).

In this work, ESTAR was used to obtain electron ranges for energies between 10 and 50 keV, to be compared with PARTRAC and MIRD electron range calculations. Uncertainties of the calculated collision stopping powers are estimated to be less than 3% in water. ESTAR radiative stopping power is not considered in this work.

RESULTS

In this section we present results for:

• PARTRAC predictions for the range of monoenergetic electrons and an analytical function to fit simulated range values as a function of energy. Range values are obtained reprocessing the output of PARTRAC calculations. The fit function is implemented for use in COOLER. PARTRAC range data are compared to MIRD and NIST-ESTAR predictions;

• the implementation in COOLER of an analytical fit function to simulated electron energy deposition data as a function of distance, and the validation of the results obtained using the function instead of the simulated energy deposition data as input for COOLER calculations;

• electron S-values as a function of energy, calculated taking the nuclear volume (N) as target region, with the following activity scenario: uniform activity in the nucleus (N←N); uniform activity in the whole cell (N←Cell); and for two different cellular geometries, simulating floating or adherent cells. S-values obtained with MIRDcell, COOLER and with full PARTRAC calculations are then compared;

• a test of the implementation in COOLER of the ^{3}H decay spectrum, together with the comparison of results obtained using the average energy instead of the whole spectrum.

ELECTRON RANGE

We calculated the electron range for energies between 5 and 50 keV reprocessing the output of PARTRAC simulations. Results can be fitted via the following equation:

$$R = 0.048 \cdot E^{1.723}, \qquad (8)$$

where R is the range in μm and E is the energy of the particle expressed in keV. Our results are compared with predictions from MIRD, which adopts Cole's formulas, and from the NIST-ESTAR database, from now on just referred to as NIST. Generally speaking, the electron range can be variously defined through concepts as the path length or the depth of penetration. The path length is the sum of all distances covered

by an electron between two successive interactions, before it loses all its energy (*50*). The maximal penetration depth is the distance between the electron starting point and the farthest interaction along a straight line. Thus, the maximal penetration depth is always shorter than the mean path length. The range in the Continuous Slowing Down Approximation (CSDA) can only be derived by taking the sum over the most probable path and assuming path length fluctuations are symmetric about the mean (*51*). To the aim of the comparison, we recall that range values are considered in MIRD as the maximal penetration depth of an electron beam fired along a single direction, once the 5% of electrons with the largest penetration depth are excluded. In COOLER electron emission is radial and only the 1% of electrons with the largest penetration depth is excluded. Fig. 3 shows MIRD's predictions along with range results obtained with PARTRAC, their fit via Eq. (8), and NIST's (CSDA) values.

Although MIRD results should refer to a “restricted” penetration depth, they closely reflect range values under the CSDA, which are larger than COOLER findings. Similar considerations were reported in (*10,17*). Such discrepancy increases with increasing energy, but it is usually negligible below 20 keV. It follows from Fig. 3 that between 5 and 50 keV, MIRD overestimates the range values up to 9.9% (equal to 3.99 μm) at 50 keV.

FIT TO ENERGY DEPOSITION MONTE CARLO DATA

COOLER offers the possibility to use analytical expressions of energy deposition versus distance instead of the Monte Carlo energy deposition data tables. This option is of clear interest, in that it allows to quickly compare results from different available energy deposition patterns, without running dedicated Monte Carlo calculations, and also for particles other than electrons. To implement and validate this option, we fitted PARTRAC energy-deposition data, then we compared the S-values calculated for different electron energies at fixed geometries, using as input the deposition data tables and the fitted functions. The proposed equation describing Monte Carlo data of energy deposition reads:

$$E_{dep}(\rho) = \frac{p_1\rho^3 + p_2\rho^2 + p_3\rho + p_4}{\rho^2 + q_1\rho + q_2}, \qquad (9)$$

where ρ is the radial distance from the point source given in μm. Eq. (9) is plotted together with its 95% confidence bounds for electrons of 5, 25 and 50 keV in Fig. 4. The goodness of the fit was evaluated through the Sum of Squares due to Error (SSE), the Adjusted R-square (R-square) and the Root Mean Squared Error (RMSE) tests. The six parameters and the statistical tests are reported in Table 2 for energies between 5 and 50 keV.

As we can notice from Fig. 4 the fit nicely reproduces the data within the 95% bounds, with the exception of the initial shoulder, whose width increases with the electrons initial energy. At 50 keV, the width of the shoulder is comparable to the cellular dimensions. This might explain the S-value discrepancies observed at the highest electron energies when comparing Eq. (9) with the PARTRAC simulated energy deposition raw data (see Table 3).

Table 2: Fit parameters

E (keV)	p1	p2	p3	p4	q1	q2	SSE	R-square	RMSE
5	0.016	-0.026	0.007	0.003	-0.825	0.260	9.0E-05	0.997	5.6E-04
10	0.009	-0.045	0.034	0.058	-2.849	2.800	3.1E-04	0.997	1.0E-03
15	0.008	-0.077	0.120	0.341	-6.113	12.240	6.6E-04	0.997	1.5E-03
20	0.002	-0.047	0.094	1.149	-9.549	30.120	1.3E-03	0.997	2.1E-03
25	0.003	-0.069	0.217	3.094	-14.470	67.550	1.9E-03	0.997	2.5E-03
30	0.002	-0.073	0.293	7.078	-20.010	129.60	3.1E-03	0.996	3.2E-03
40	0.001	-0.101	0.707	25.640	-33.410	359.50	4.7E-03	0.997	4.0E-03
50	0.001	-0.080	0.363	71.040	-49.600	773.60	6.2E-03	0.997	4.6E-03

Notes. Eq. (9) parameters are reported for different energies, spacing from 5 to 50 keV. The goodness of the model was evaluated through the Sum of Squares due to Error (SSE), the Adjusted R-square (R-square) and the Root Mean Squared Error (RMSE) tests.

Table 3: S-value comparison between PARTRAC raw data and Eq. (9)

	Floating - Eq. (9)	Floating - PARTRAC	Adherent - Eq. (9)	Adherent - PARTRAC
E (keV)	S (Gy/decay)	S (Gy/decay)	S (Gy/decay)	S (Gy/decay)
5	5.34E-04	5.34E-04	5.50E-04	5.51E-04
10	1.10E-03	1.10E-03	1.10E-03	1.10E-03
15	1.50E-03	1.50E-03	1.40E-03	1.40E-03
20	1.70E-03	1.70E-03	1.50E-03	1.50E-03
25	1.60E-03	1.60E-03	1.30E-03	1.30E-03
30	1.20E-03	1.20E-03	1.10E-03	1.10E-03
40	7.90E-04	8.08E-04	6.85E-04	6.98E-04
50	5.77E-04	6.10E-04	4.98E-04	5.27E-04

Notes. A comparison of S-values, obtained using Eq. (9) and PARTRAC energy deposition data, is presented for floating and adherent V79 cells. Initial energies range from 5 to 50 keV.

S-VALUES CALCULATION

The four panels in Fig. 5 show a comparison of S-values as a function of electron energy obtained through three different tools: COOLER (orange, in panels from A to D), PARTRAC (grey, in panels from A to C) and MIRDcell V2.0.15 software (*43*) (blue, in panels A and B). PARTRAC error bars are standard deviations from five independent simulation runs with a statistic of 5000 tracks each. In panels A and C the source region is the cell nucleus (N), in panels B and D the entire cell. The target region is always the nucleus. The geometrical parameters of the two cellular configurations simulate V79 cells in suspension (A and B) or adherent culture condition (C and D). Since MIRD S-values can be computed only for spherical geometries, the comparison with MIRDcell is not possible for adherent cells, where the cell nucleus is modelled as an ellipsoid. Since the shape of the whole cell in adherent culture is modelled as a portion of ellipsoid (Fig. 2), only COOLER calculations are easily available in this case and shown in panel D. When we deal with the N←N case, the cellular shape is of no interest, as the activity is entirely contained in the nucleus, and both COOLER and PARTRAC can be used for V79 adherent cells.

From the results in panels A-C of Fig. 5, we can state that the convolution method implemented in COOLER is able to satisfactorily reproduce the results of full Monte Carlo calculations with PARTRAC, for all geometrical configuration and electron energies.

The role of geometry can be singled out in explaining the deviations still observed, as *e.g.* in panel B at 25 keV: as it is shown in Fig. 4 for 25 keV electrons, there is indeed a pronounced peak in the energy-deposition curve at approximately 6 μm, which is close to the radius of V79 cell nucleus model.

Concerning the higher energy tails, the higher the electron energy the lower the accuracy of the density matrix built in COOLER. This approximation therefore plays a role in the disagreement between PARTRAC and COOLER at 40 and 50 keV in panels A and B.

The most important results presented in Fig. 5 concern the comparison of COOLER and PARTRAC predictions to MIRDCell results. For the sake of this comparison, we need to take into account the

existence of an unavoidable source of disagreement at all energies, due to the geometrical approximations required by MIRDcell (which accepts only integer numbers for geometrical parameters of the cell). However, observed discrepancies are large only in the intermediate energy range, which suggests that differences in the shape of energy deposition curves are to be considered as the main cause.

Generally speaking, a good agreement among all tools was expected below 10 keV, because of the short range of low energy electrons, which makes that only electrons originating in the nucleus contribute to the nuclear dose. A good agreement is revered for the highest electron energies, where the dependency on the shape of the energy-deposition curve is weaker (if, as in our case, we neglect cross-dose effects between neighboring cells): at 50 keV the deposition peak is found at a distance of approximately 20 μm, far outside the cell itself (see again Fig. 4).

In the two source-target configurations the N←Cell case always presents smaller S-values than N←N. The reason is simply found in the increased volume of the source region for the N←Cell case. As already discussed, the activity normalization factor increases with the volume of the source region.

Cell geometrical parameters are based on experimental measurements. In this way, we created reliable average configurations for V79 cells in different culture conditions. In Fig. 6 we report S-value calculations for adherent V79 cells for different positions of the cell nucleus: Pos1 is the default setting, with a 1.4 μm thickness of cytoplasm beneath the cell nucleus (see (*35*) and Material and Methods); Pos2 corresponds to a nucleus at an intermediate vertical position, with a 0.7 μm distance between the mylar base and the bottom of the nucleus; Pos3 represents the less realistic situation, in which the nucleus lays on the bottom of the cell touching the mylar surface. Changes in S-values are observed depending on the nuclear position in the energy range 15 - 30 keV, with differences up to 15%, found to be maximal at 25 keV. For the same reasons given when we compared COOLER to MIRDCell results, no change is seen below 10 keV, which is due to the short electron range. A small and negligible S-value dependence on the positioning of the nucleus is observed at 40 and 50 keV, where the energy deposition peak is far outside

the cell. This set of results is included in order to stress the importance of modelling the nuclear position correctly.

THE ^{3}H CASE

We computed S-values in the N←Cell activity scenario comparing results obtained with the use of tritium beta-decay spectrum and of its mean energy. Adopting the spherical geometry for V79 cells in suspension, we obtained the following S-values: $6.08 \cdot 10^{-4}$ Gy/decay for the full spectrum and $6.07 \cdot 10^{-4}$ Gy/decay using only the mean energy. The chosen modelling conditions allows us to assume totally uniform energy deposition in the medium. Under these circumstances we do not have to care about nuclear dimensions, since the deposited energy increases with the nuclear size, so that the S-value remains constant. In other words, a second cell with radial dimensions equal to 1 and 8 μm would still provide the same result for the S-value. These conditions hide the differences in the use of the full spectrum or just the mean energy. Experimentally, such condition can often be reached through a uniform distribution of the activity, which is the case of tritiated water.

CONCLUSIONS

Absorbed dose calculations in nuclear medicine are conventionally based on the formalism of the S-values introduced by the MIRD committee. The integral method adopted for low energy electron emitters has some well-known limitations, as the employment of Cole's effective stopping power, the assumption of CSDA and the use of geometric reduction factors, which can be easily calculated only for simple geometries. These limitations suggest that Monte Carlo codes with low energy cut-offs for electron transport and more degrees of freedom in the geometry implementation are more suitable for S-value calculations. Among Monte Carlo programs, event by event codes like PARTRAC, should be preferred to condensed-history codes for cellular S-value calculations.

Common concerns related to Monte Carlo simulations are typically: the computing time, the availability of the program and the possibility to implement new functions from scratch as, for example, cellular geometries or activity distributions, which is often far from being trivial. Thus, on one hand Monte Carlo codes can provide accurate S-values, on the other hand they are normally beyond the practical reach of the preclinical and clinical researcher. For such reasons we decided to develop the analytical tool COOLER for calculations of electron energy deposition at the sub-cellular level, which employs PARTRAC results as input and is validated through dedicated full Monte Carlo calculations. The adopted method can be extended to electrons (and in principle other particles) of any energy of interest and to geometries where the geometrical reduction factors do not exist or may be ill defined.

Values for the range of electrons are defined in this work as the maximal penetration depth of electrons emitted isotropically from a point source in water, once the 1% of electrons with the largest penetration depths are excluded to avoid the influence of statistical outliers. Range values were obtained in PARTRAC and implemented in COOLER through an analytical fit function. Such values were compared to MIRD and NIST-ESTAR predictions. Looking at the range results, discrepancies between MIRD (Cole) and COOLER (PARTRAC) increase with the energy, but are usually negligible below 20 keV and

COOLER range values are up to 6.76% shorter than MIRD findings at 50 keV. MIRD results are always in good agreement with the NIST-ESTAR predictions. However, we cannot perform an accurate comparison between MIRD and COOLER, as they take advantage of different geometrical setups and different range definitions. NIST-ESTAR predictions are theoretically derived from Bethe's theory.

To promote the use of COOLER, we implemented realistic geometries for the chosen V79 cell model in two different culture conditions, namely a spherical geometry for free-floating cells and a quasi-ellipsoidal configuration for cells growing as monolayers on plastic surfaces.

The approach adopted in COOLER for S-value calculations lies on the convolution of two main terms: the first is related to the distribution of electron sources in different cellular compartments; the second, which is derived from PARTRAC simulations, to the density of deposited energy in liquid water as a function of the radial distance from the source. This direct convolution method is validated against full PARTRAC simulations.

The largest discrepancies between COOLER and MIRD generally arise for electrons at around 25 keV and the difference can be as high as 60%. For V79 cells, energy deposition results for electrons in the range of 15 - 25 keV present the highest dependence on the geometry, due to the non-linear shape of the deposited energy versus distance curve. For these energies deposition peaks are located between 2.5 and 6 μm; such distances are comparable with the radial dimensions of the cells. We recommend to pay extra attention when modelling the position of the target. In our simulations for V79 adherent cells, the ambiguous positioning of the cell nucleus led to discrepancy in the S-values up to 15%.

COOLER is not pegged to PARTRAC and can work with any Monte Carlo code. An easy way to compare results between COOLER and other programs consists in selecting as input for COOLER analytical expressions for the deposited energy as a function of radial distance obtained from different Monte Carlo codes. In this work, we also have provided an example of analytical equation to fit PARTRAC energy-deposition data for electrons.

COOLER is developed starting from monoenergetic electron sources, but it can also accept beta decay spectra. In this work, we have shown as an example how COOLER handles the use of the continuous electron energy distribution resulting from tritium decay. In particular, the same S-value is found regardless of the use of the tritium spectrum or of its mean energy. As tritiated water freely diffuses in all cell compartments, leading to uniform activity distributions, and due to the emission of solely short range electrons, all calculations were carried out under totally uniform energy deposition conditions. From such calculations we argue that in many experimental situations, involving low energy electron emitters, information on the full decay spectrum is not needed, as uniform energy deposition conditions are granted and the use of the mean energy is often sufficient to the scope. Experimentally, such condition can often be reached through a uniform distribution of the activity, which is the case of tritiated water.

In this work, we have established a new analytical method to calculate energy deposition by electrons at the sub-cellular level, avoiding the shortenings related to Cole's formula for the electron stopping power and the use of geometric reduction factors. The tool we provide is demonstrated to handle correctly a variety of cell geometries, taking as input analytical fit functions for electron range values and energy deposition data obtained from Monte Carlo calculations. COOLER provides the best possible expression of cellular S-values, limited only to the precision by which the cellular geometry can be described. The use of COOLER is much simpler than the use of a Monte Carlo code and this makes it useful both for scientists and the medical personnel concerned with S-value calculations. The software will be made available for download from DTU-Nutech website: http://www.nutech.dtu.dk/.

ACKNOWLEDGMENTS

Authors are grateful to staff scientists and technicians of the Hevesy laboratory at the Technical University of Denmark and the scientists of the Radiobiology and Radiation Biophysics group of the University of Pavia.

LISTING OF THE FIGURE LEGENDS

Fig. 1

30 keV electron tracks generated in liquid water using the Monte Carlo code PARTRAC. At the top (A), the experimental set-up adopted by Cole (*19*) and MIRD (1). At the bottom (B), the particle emission mode used in this work to determine the deposited energy against distance interrelations.

Fig.2

Schematic representations of the cellular geometries included in COOLER. V79 cells in suspension (panel A) have a nuclear radius of 5.2 μm and a cellular radius of 7.1 μm. V79 adherent cells are illustrated in panel B. The thickness of the nucleus is 6.6 μm, the thickness of cytoplasm between the mylar base and the cell nucleus is 1.4 μm. The amount of cytoplasm above the nucleus is fixed at 175 nm. The projection of the nuclear area on the mylar base is 134 μm^2, while the nuclear and cellular volumes are assumed to be the same in A and B, namely 1500 μm^3.

Fig.3

The energy versus range dependence obtained by Cole (*19*), adopted by MIRD (*1*) and presented in Eq. (5) is shown as a blue line. Such relationship is in good agreement with NIST (*45*) range values, which are given only for energies above 10 keV (grey line). COOLER range values are shown in orange and given by Eq. (8). Triangles represent PARTRAC simulated range values.

Fig.4

Eq. (9) to fit PARTRAC energy-deposition data (dots) as a function of distance is shown as a black line together with its 95% confidence bounds for three different initial energies, respectively 5 (A), 25 (B) and 50 (C) keV.

Fig.5

The four panels show a comparison of S-values for monoenergetic electrons obtained through three different tools: MIRDcell software (blue) (*43*), PARTRAC (grey) and COOLER (orange). PARTRAC error bars are standard deviations of five independent simulations containing 5000 tracks each. Source regions change from the cell nucleus (N) to the entire cell. The target region is always N. Panel A shows S-values for V79 cells in suspension containing radioactivity only in the cell nucleus (N). Panel B maintains the geometrical structure of A, while the activity is uniformly distributed in the whole cell. Panel C shows S-values for adherent V79 cells, whose activity is present just in the nucleus. In panel (D), the activity is uniformly distributed everywhere in the cell. As the cell nucleus is modelled as an ellipsoid, MIRDcell cannot be used in C and D. As the cell is modelled as a portion of ellipsoid, only COOLER can be used in D.

Fig.6

Dependency of S-value calculations from cell nucleus position within V79 adherent cells is shown. Geometrical volumes are kept constant, while only the vertical position of the cell nucleus is changed. In Pos1 the amount of cytoplasm beneath the cell nucleus corresponds to 1.4 μm. Pos2 indicates that the nucleus floats at an intermediate vertical position with a 0.7 μm distance between the mylar base and the bottom of the nucleus. In Pos3 the nucleus lays on the bottom of the cell.

REFERENCES

1. Goddu SM, Howell RW, Bouchet LG, Bolch WE, Rao D V. MIRD cellular S values. Reston, VA Soc Nucl Med. 1997;

2. Kassis AI. The MIRD approach: remembering the limitations. J Nucl Med. 1992;33(5):781–2.

3. Howell RW. The MIRD schema: from organ to cellular dimensions. J Nucl Med. 1994;35(3):531–3.

4. Makrigiorgos GM, Ito S, Baranowska-Kortylewicz J, Vinter DW, Iqbal A. Inhomogeneous Deposition of Radiopharmaceuticals at the Cellular Level. J Nucl Med. 1990;31(8):1358-63

5. Makrigiorgos GM, Baranowska-Kortylewicz J, den Abbeele AD, Ito S, Vinter DW, Adelstein SJ, et al. Microscopic spatial inhomogeneity of radiopharmaceutical deposition in mammalian tissues: dosimetry at the cellular level and comparison with conventional dosimetry. Radiat Prot Dosimetry. 1990;31(1–4):319–24.

6. Griffiths GL, Govindan S V, Sgouros G, Ong GL, Goldenberg DM, Mattes MJ. Cytotoxicity with Auger electron-emitting radionuclides delivered by antibodies. Int J cancer. 1999;81(6):985–92.

7. Neti PVS V, Howell RW. Log normal distribution of cellular uptake of radioactivity: implications for biologic responses to radiopharmaceuticals. J Nucl Med. 2006;47(6):1049–58.

8. Kriehuber R, Riedling M, Simkó M, Weiss DG. Cytotoxicity, genotoxicity and intracellular distribution of the Auger electron emitter 65Zn in two human cell lines. Radiat Environ Biophys. 2004;43(1):15–22.

9. Kassis AI. Therapeutic radionuclides: biophysical and radiobiologic principles. In: Seminars in nuclear medicine. 2008. p. 358–66.

10. Emfietzoglou D, Bousis C, Hindorf C, Fotopoulos A, Pathak A, Kostarelos K. A Monte Carlo

study of energy deposition at the sub-cellular level for application to targeted radionuclide therapy with low-energy electron emitters. Nucl Instruments Methods Phys Res Sect B Beam Interact with Mater Atoms. 2007;256(1):547–53.

11. Kassis AI. The amazing world of Auger electrons. Int J Radiat Biol. 2004;80(11–12):789–803.

12. Fischer T, Schomäcker K, Schicha H. Diethylstilbestrol (DES) labeled with Auger emitters: Potential radiopharmaceutical for therapy of estrogen receptor-positive tumors and their metastases? Int J Radiat Biol. 2008;84(12):1112–22.

13. Yasui LS. Molecular and cellular effects of Auger emitters: 2008--2011. Int J Radiat Biol. 2012;88(12):864–70.

14. Kassis AI. Molecular and cellular radiobiological effects of Auger emitting radionuclides. Radiat Prot Dosimetry. 2010;ncq385.

15. Kassis AI. Cancer therapy with Auger electrons: Are we almost there? J Nucl Med. 2003;44(9):1479–81.

16. Bambynek W, Crasemann B, Fink RW, Freund H-U, Mark H, Swift CD, et al. X-ray fluorescence yields, Auger, and Coster-Kronig transition probabilities. Rev Mod Phys. 1972;44(4):716.

17. Emfietzoglou D, Kostarelos K, Hadjidoukas P, Bousis C, Fotopoulos A, Pathak A, et al. Subcellular S-factors for low-energy electrons: a comparison of Monte Carlo simulations and continuous-slowing-down calculations. Int J Radiat Biol. 2008;84(12):1034–44.

18. Howell RW, Rao D V, Sastry KSR. Macroscopic dosimetry for radioimmunotherapy: nonuniform activity distributions in solid tumors. Med Phys. 1989;16(1):66–74.

19. Cole A. Absorption of 20-eV to 50,000-eV electron beams in air and plastic. Radiat Res. 1969;38(1):7–33.

20. Nikjoo H. Auger electron transport calculations in biological matter. 2013;

21. Nikjoo H, Uehara S, Emfietzoglou D, Cucinotta FA. Track-structure codes in radiation research. Radiat Meas. 2006;41(9):1052–74.

22. MATLAB. version 8.5.0.197613 (R2015a). The MathWorks Inc.; 2015.

23. Bousis C, Emfietzoglou D, Hadjidoukas P, Nikjoo H. A Monte Carlo study of cellular S-factors for 1 keV to 1 MeV electrons. Phys Med Biol. 2009;54(16):5023.

24. Hartman T, Lundqvist H, Westlin J-E, Carlsson J. Radiation doses to the cell nucleus in single cells and cells in micrometastases in targeted therapy with 131 I labeled ligands or antibodies. Int J Radiat Oncol Biol Phys. 2000;46(4):1025–36.

25. Stewart RD, Wilson WE, McDonald JC, Strom DJ. Microdosimetric properties of ionizing electrons in water: a test of the PENELOPE code system. Phys Med Biol. 2001;47(1):79.

26. Coulot J, Ricard M, Aubert B. Validation of the EGS usercode DOSE3D for internal beta dose calculation at the cellular and tissue levels. Phys Med Biol. 2003;48(16):2591.

27. Syme AM, Kirkby C, Riauka TA, Fallone BG, McQuarrie SA. Monte Carlo investigation of single cell beta dosimetry for intraperitoneal radionuclide therapy. Phys Med Biol. 2004;49(10):1959.

28. Hindorf C, Emfietzoglou D, Lindén O, Kostarelos K, Strand S-E. Internal microdosimetry for single cells in radioimmunotherapy of B-cell lymphoma. Cancer Biother Radiopharm. 2005;20(2):224–30.

29. Hindorf C, Emfietzoglou D, Lindén O, Bousis C, Fotopoulos A, Kostarelos K, et al. Single-cell dosimetry for radioimmunotherapy of B-cell lymphoma patients with special reference to leukemic spread. Cancer Biother Radiopharm. 2007;22(3):357–66.

30. Pacilio M, Lanconelli N, Meo S Lo, Betti M, Montani L, Aroche LAT, et al. Differences among

Monte Carlo codes in the calculations of voxel S values for radionuclide targeted therapy and analysis of their impact on absorbed dose evaluations. planning. 2009;5:8.

31. Friedland W, Dingfelder M, Kundrát P, Jacob P. Track structures, DNA targets and radiation effects in the biophysical Monte Carlo simulation code PARTRAC. Mutat Res Mol Mech Mutagen. 2011;711(1):28–40.

32. Dingfelder M, Hantke D, Inokuti M, Paretzke HG. Electron inelastic-scattering cross sections in liquid water. Radiat Phys Chem. 1999;53(1):1–18.

33. Dingfelder M, Ritchie RH, Turner JE, Friedland W, Paretzke HG, Hamm RN. Comparisons of calculations with PARTRAC and NOREC: transport of electrons in liquid water. Radiat Res. 2008;169(5):584–94.

34. Alloni D, Campa A, Friedland W, Mariotti L, Ottolenghi A. Track structure, radiation quality and initial radiobiological events: Considerations based on the PARTRAC code experience. Int J Radiat Biol. 2012;88(1–2):77–86.

35. Ottolenghi A. FM, M. Merzagora A. A Monte Carlo calculation of cell inactivation by light ions. Int J Radiat Biol. 1997;72(5):505–13.

36. Townsend KMS, Stretch A, Stevens DL, Goodhead DT. Thickness measurements on V79-4 cells: A comparison between laser scanning confocal microscopy and electron microscopy. Int J Radiat Biol. 1990;58(3):499–508.

37. Townsend KMS, Marsden SJ. Nuclear area measurement on viable cells, using confocal microscopy. Int J Radiat Biol. 1992;61(4):549–51.

38. Bettega P. Calzolari SM Doglia B. Dulio L. Tallone AM Villa D. Technical report: cell thickness measurements by confocal fluorescence microscopy on C3H10T1/2 and V79 cells. Int J Radiat Biol. 1998;74(3):397–403.

39. Eckerman KF, Sjoreen AL. Rad Toolbox User's Guide. 2013.

40. Eckerman K, Endo A. ICRP Publication 107. Nuclear decay data for dosimetric calculations. Ann ICRP. 2007;38(3):7–96.

41. European Commission Radiation Protection. Emerging issues on tritium and low energy beta emitters. Report No. 152. Proceedings of the EU Scientific Seminar; 2007; Luxembourg. Available from: http://ec.europa.eu/energy/nuclear/radiation_protection/doc/publication/152.pdf

42. Alloni D, Cutaia C, Mariotti L, Friedland W, Ottolenghi A. Modeling Dose Deposition and DNA Damage Due to Low-Energy β^- Emitters. Radiat Res. 2014;182(3):322–30.

43. Vaziri B, Wu H, Dhawan AP, Du P, Howell RW, Bolch WE, et al. MIRD pamphlet no. 25: MIRDcell V2. 0 software tool for dosimetric analysis of biologic response of multicellular populations. J Nucl Med. 2014;55(9):1557–64.

44. Bolch WE, Eckerman KF, Sgouros G, Thomas SR. MIRD pamphlet no. 21: a generalized schema for radiopharmaceutical dosimetry - standardization of nomenclature. J Nucl Med. 2009;50(3):477–84.

45. Berger MJ. ESTAR, PSTAR, and ASTAR: Computer programs for calculating stopping-power and range tables for electrons, protons, and helium ions. Unknown. 1992;

46. Bethe H. Zur theorie des durchgangs schneller korpuskularstrahlen durch materie. Ann Phys. 1930;397(3):325–400.

47. Bethe H. Bremsformel für elektronen relativistischer geschwindigkeit. Zeitschrift für Phys. 1932;76(5–6):293–9.

48. Sternheimer RM. The density effect for the ionization loss in various materials. Phys Rev. 1952;88(4):851.

49. Sternheimer RM, Seltzer SM, Berger MJ. Density effect for the ionization loss of charged particles in various substances. Phys Rev B. 1982;26(11):6067.

50. Attix FH. Introduction to radiological physics and radiation dosimetry. John Wiley & Sons; 2008.

51. Berger M, Seltzer S. 10. Tables of energy-losses and ranges of electrons and positrons. Stud penetration Charg Part matter. 1964;(39):205.

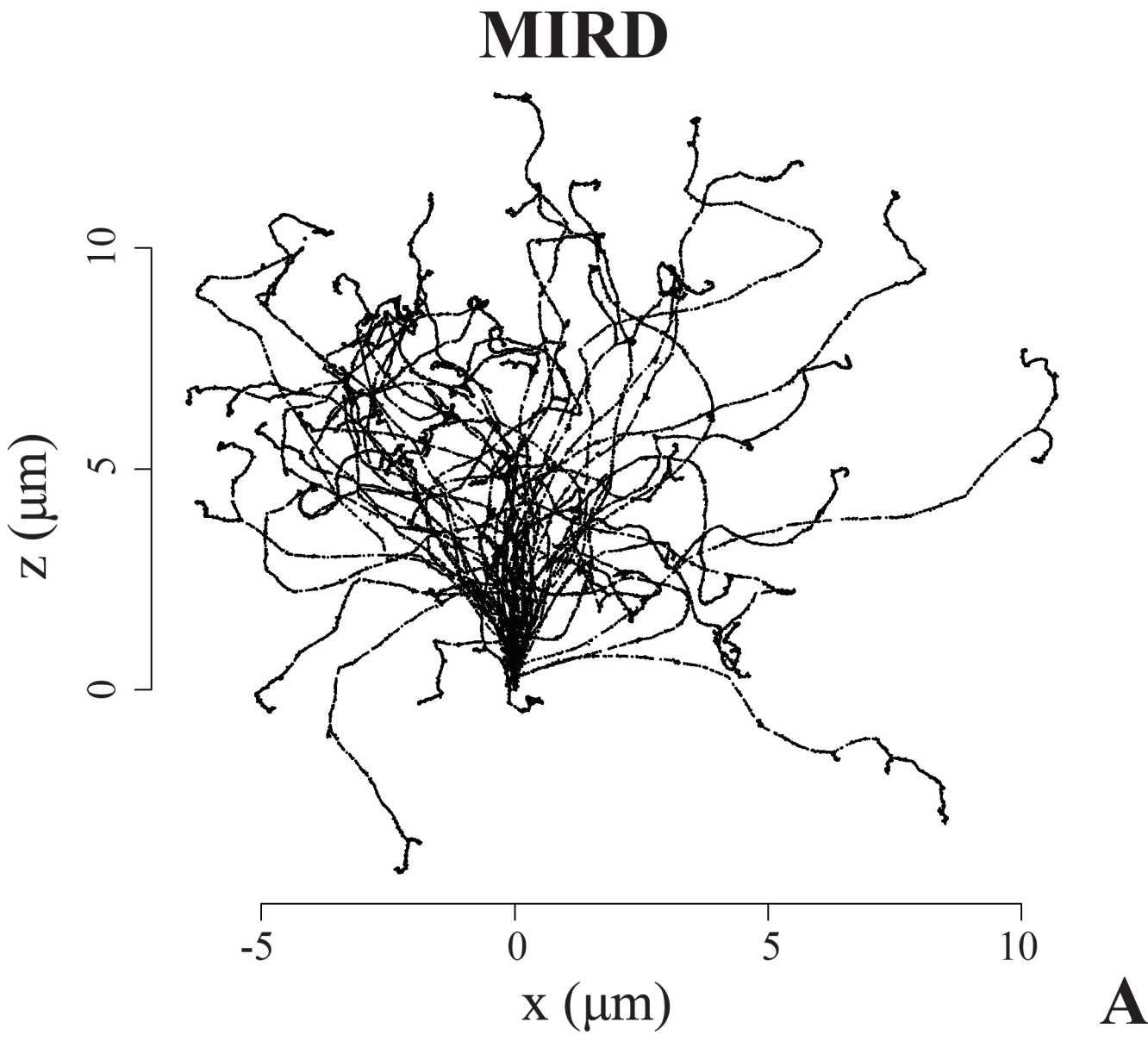
MIRD
z (μm)
10
5
0
-5
0
5
10
x (μm)
A

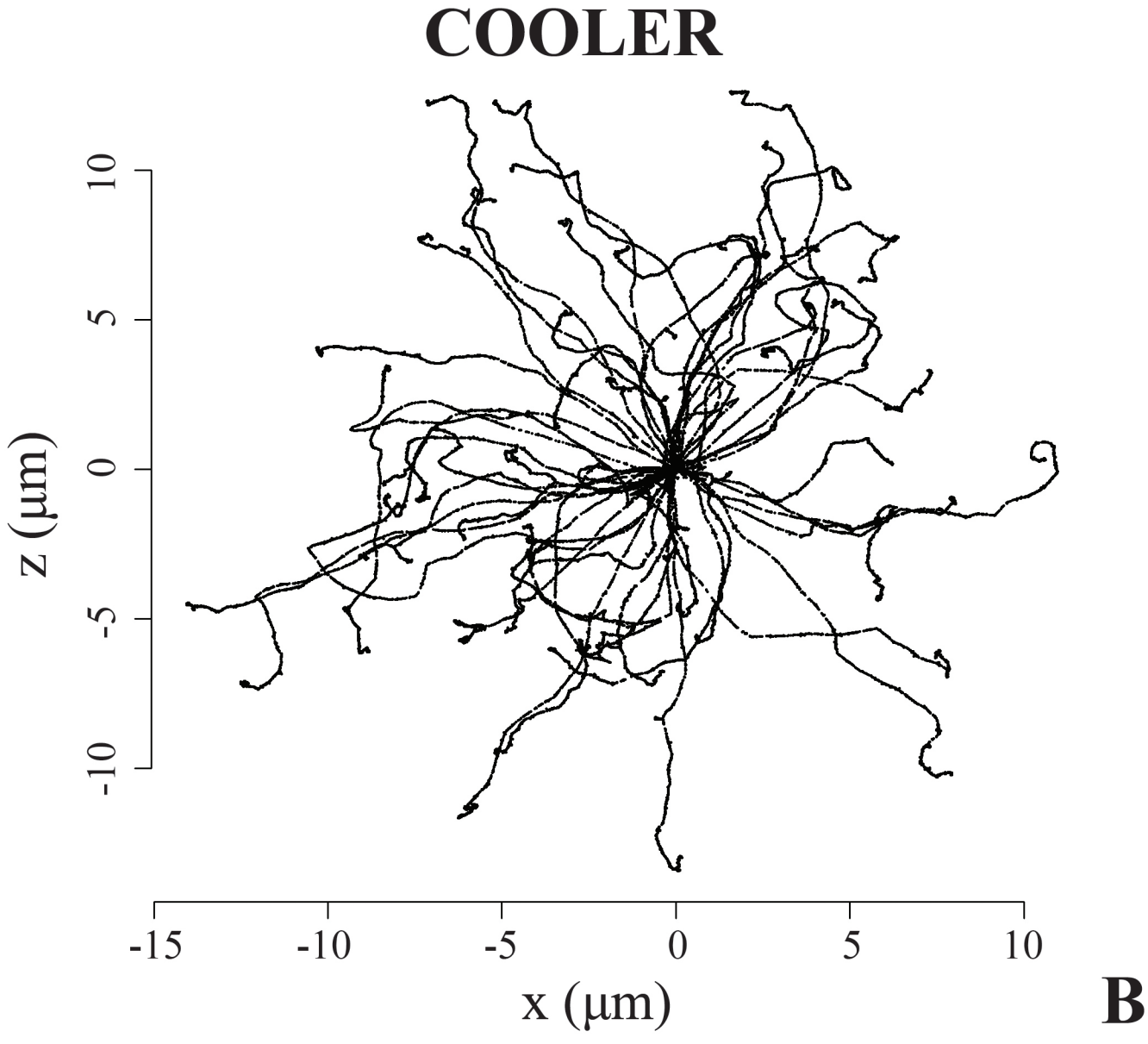
COOLER
z (μm)
10
5
0
-5
-10
-15
-10
-5
0
5
10
x (μm)
B

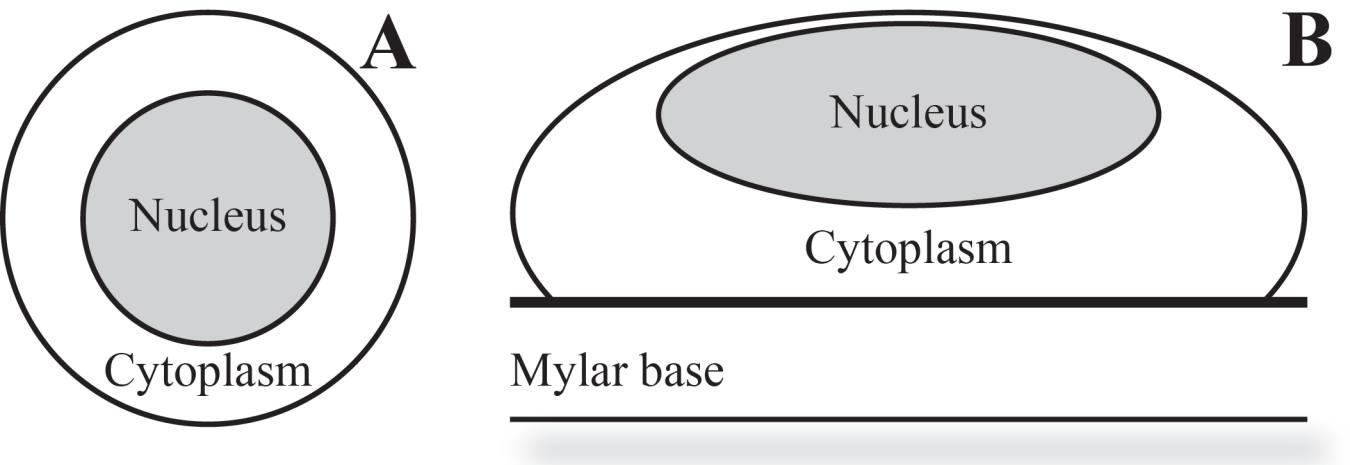
A
Nucleus
Cytoplasm
B
Nucleus
Cytoplasm
Mylar base

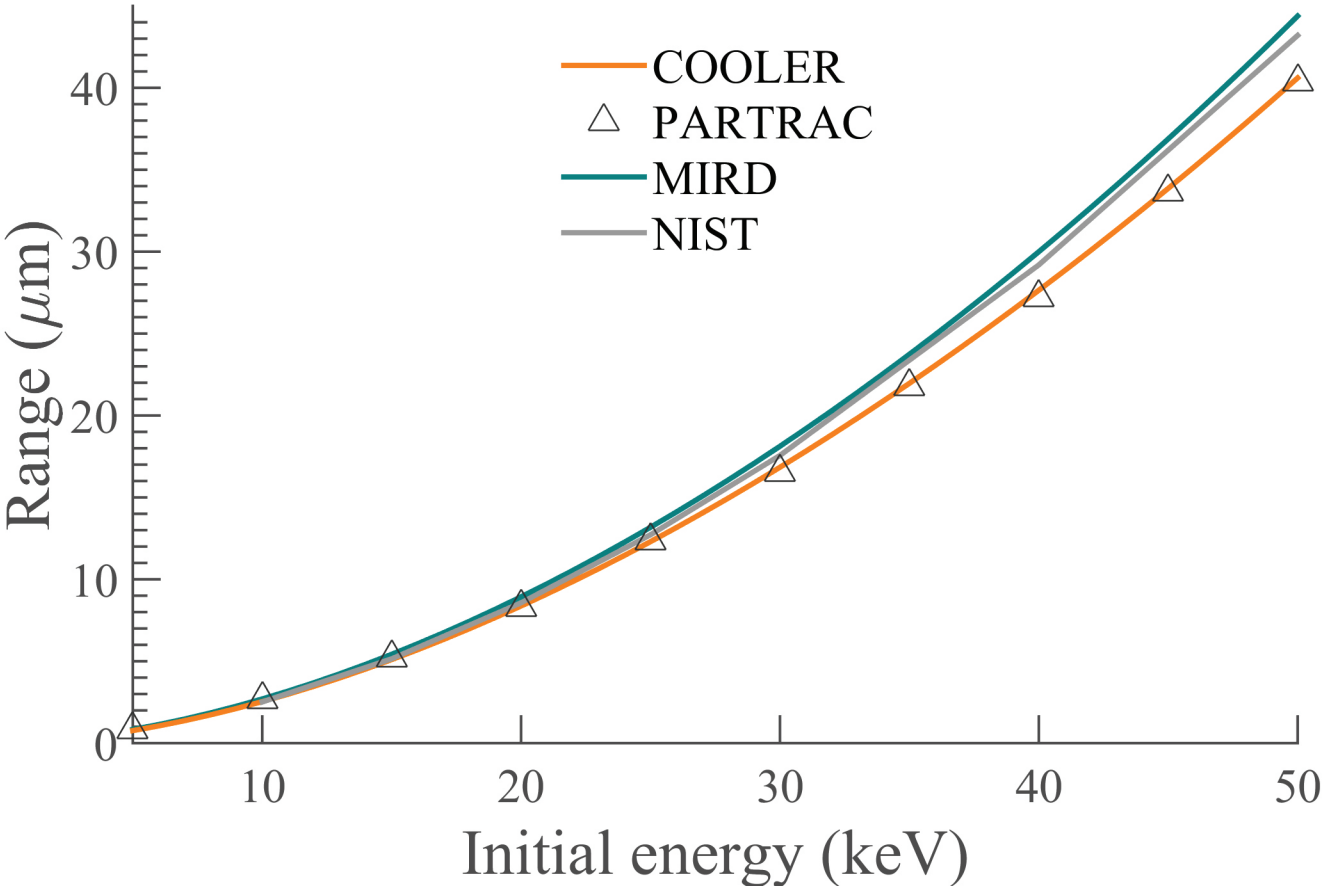
COOLER
PARTRAC
MIRD
NIST
Range (μm)
0
10
20
30
40
10
20
30
40
50
Initial energy (keV)

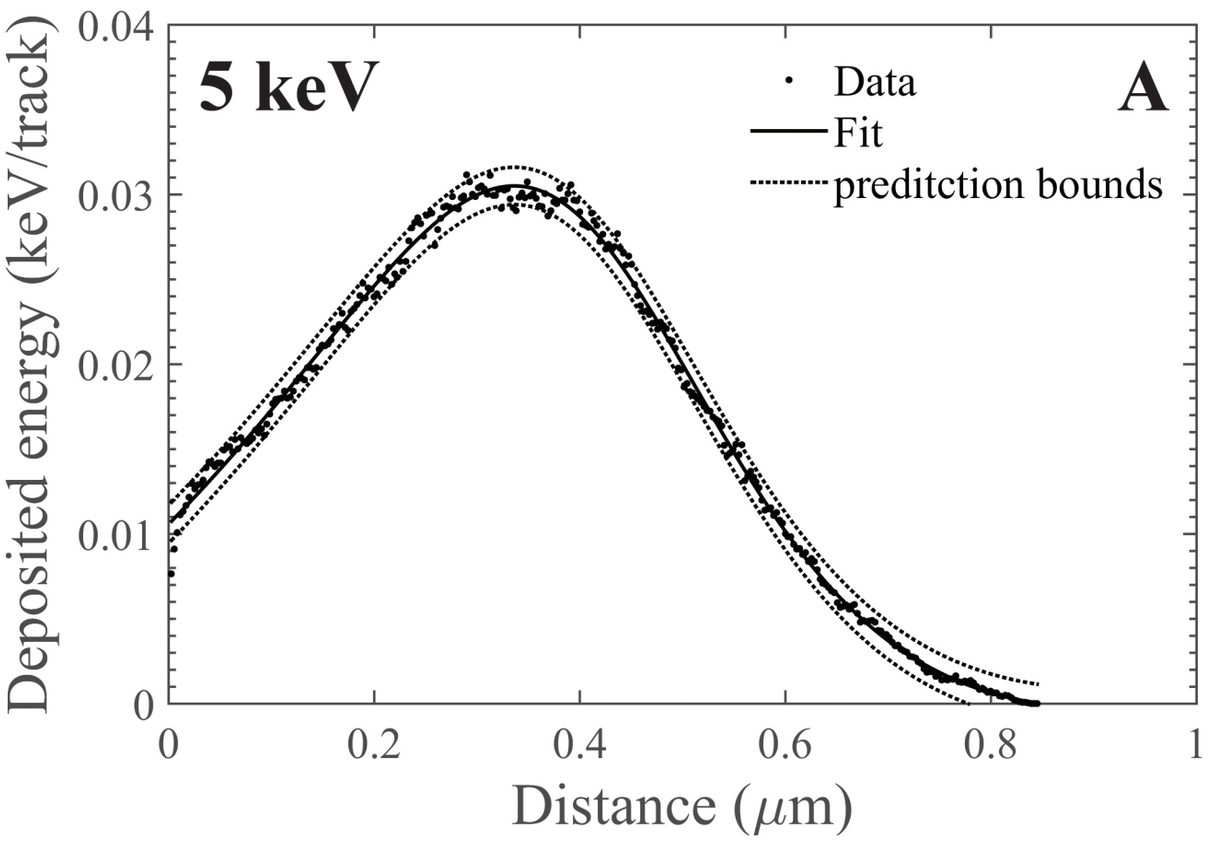
5 keV
A
Data
Fit
preditction bounds
Deposited energy (keV/track)
0.04
0.03
0.02
0.01
0
0
0.2
0.4
0.6
0.8
1
Distance (μm)

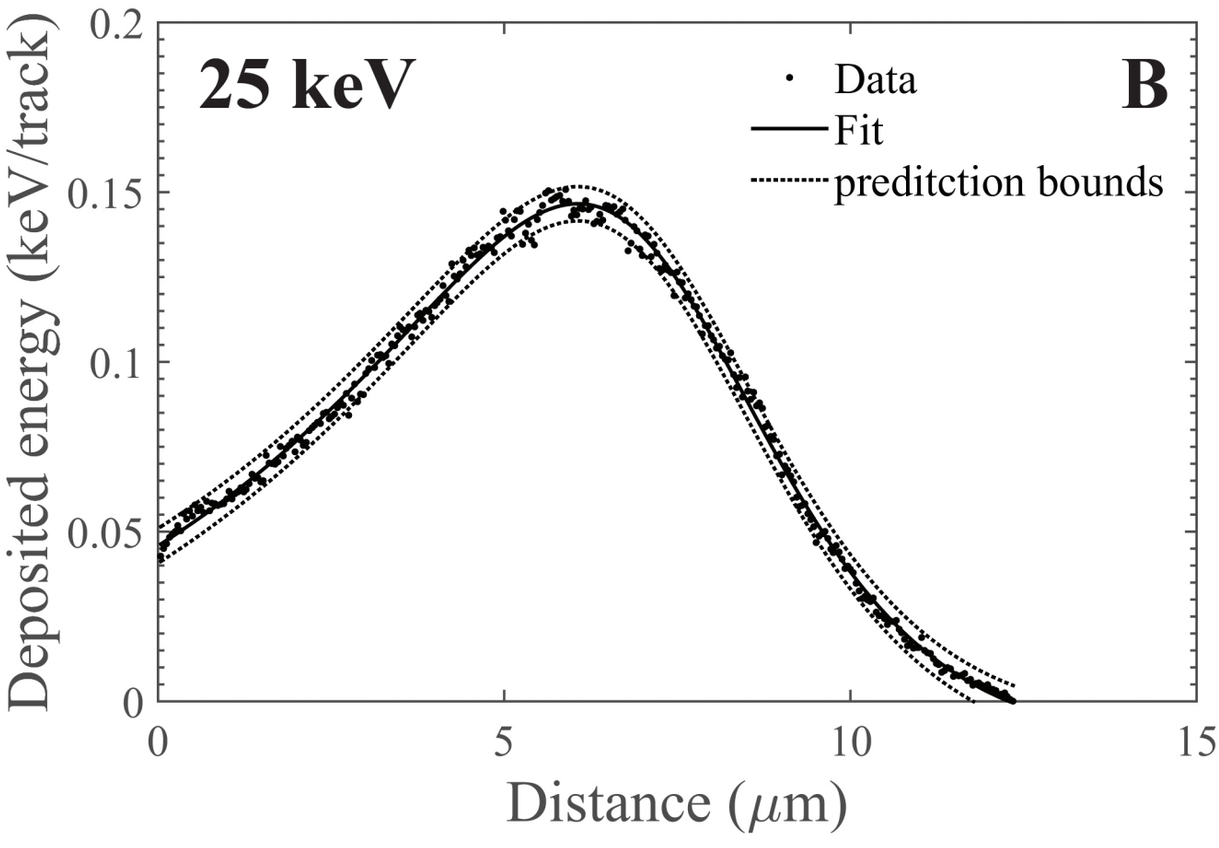
25 keV
B
Data
Fit
preditction bounds
Deposited energy (keV/track)
0.2
0.15
0.1
0.05
0
0
5
10
15
Distance (μm)

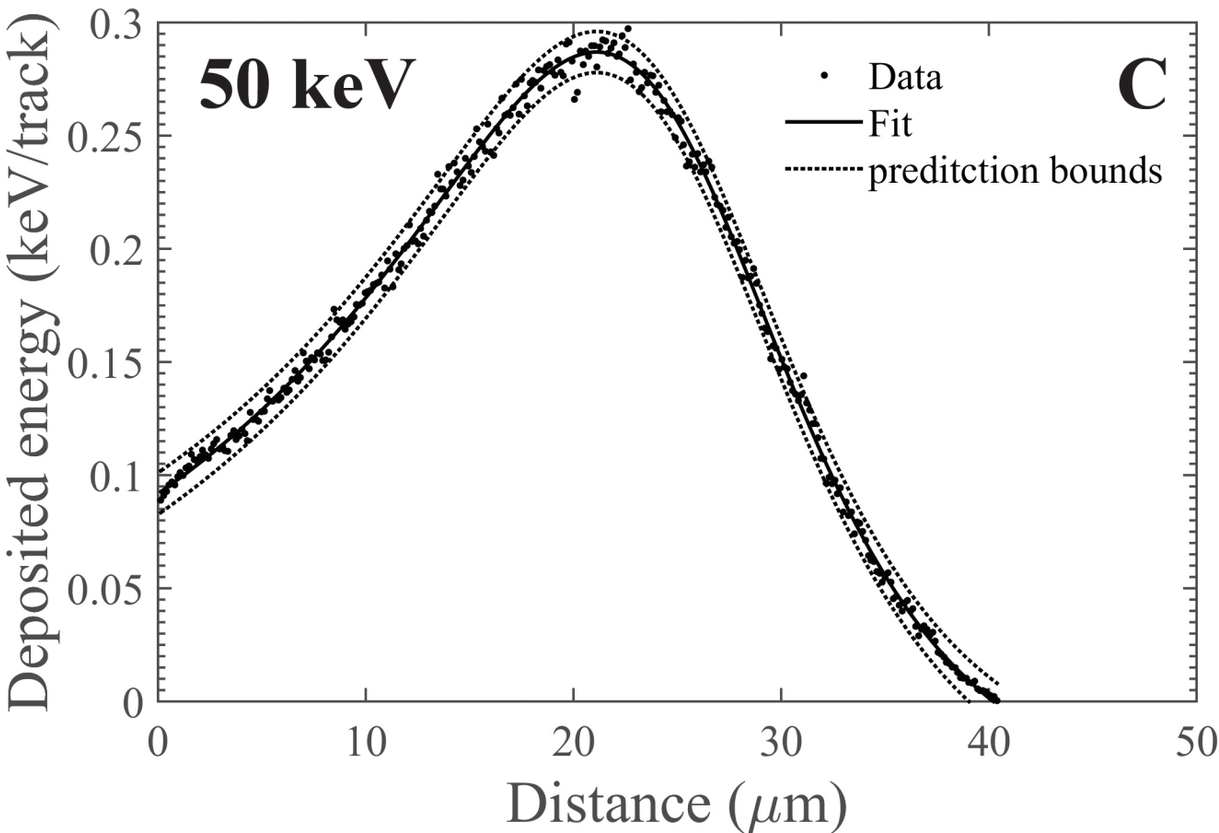
50 keV
C
Data
Fit
preditction bounds
Deposited energy (keV/track)
0.3
0.25
0.2
0.15
0.1
0.05
0
0
10
20
30
40
50
Distance (μm)

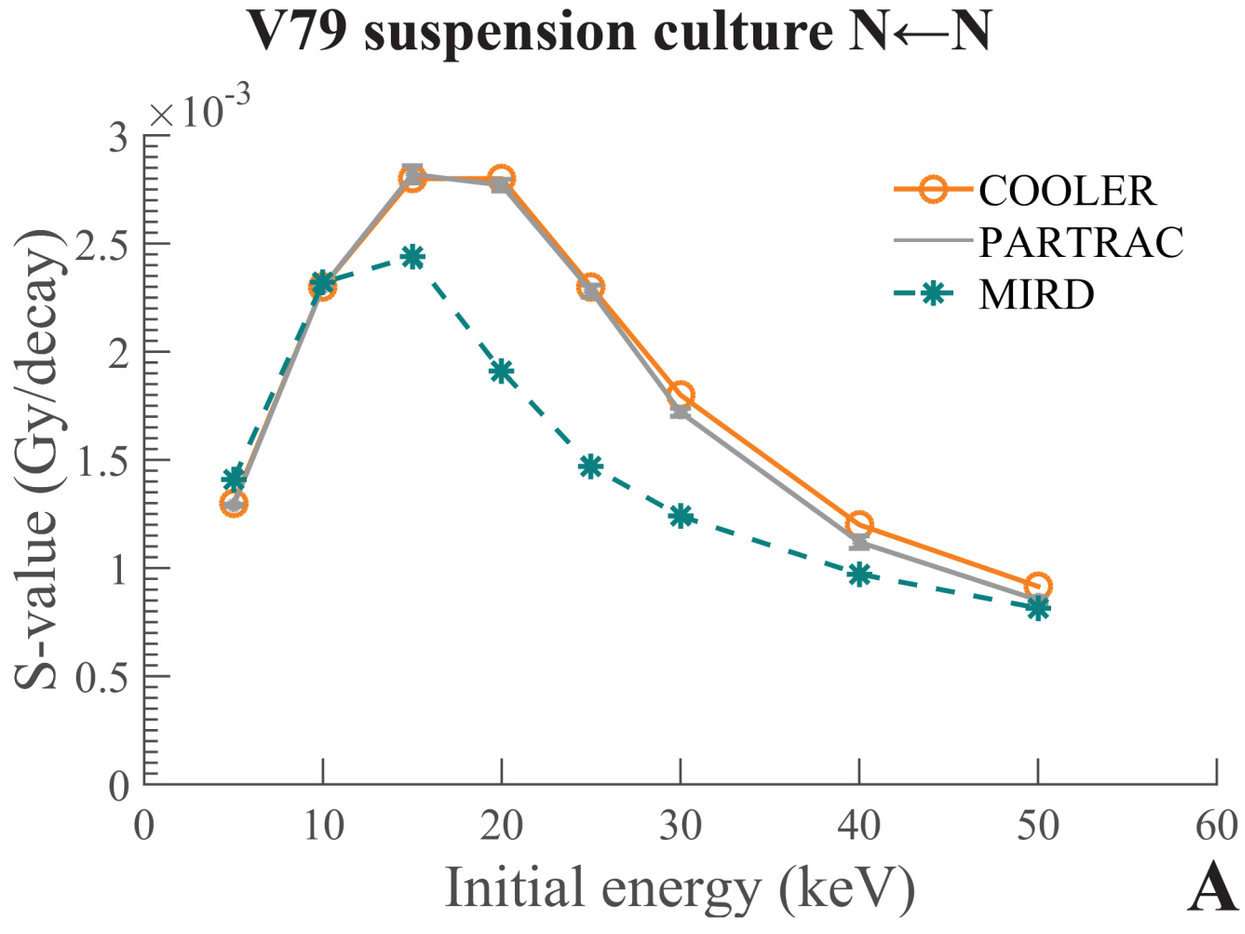
V79 suspension culture N←N
×10-3
S-value (Gy/decay)
Initial energy (keV)
COOLER
PARTRAC
MIRD
A

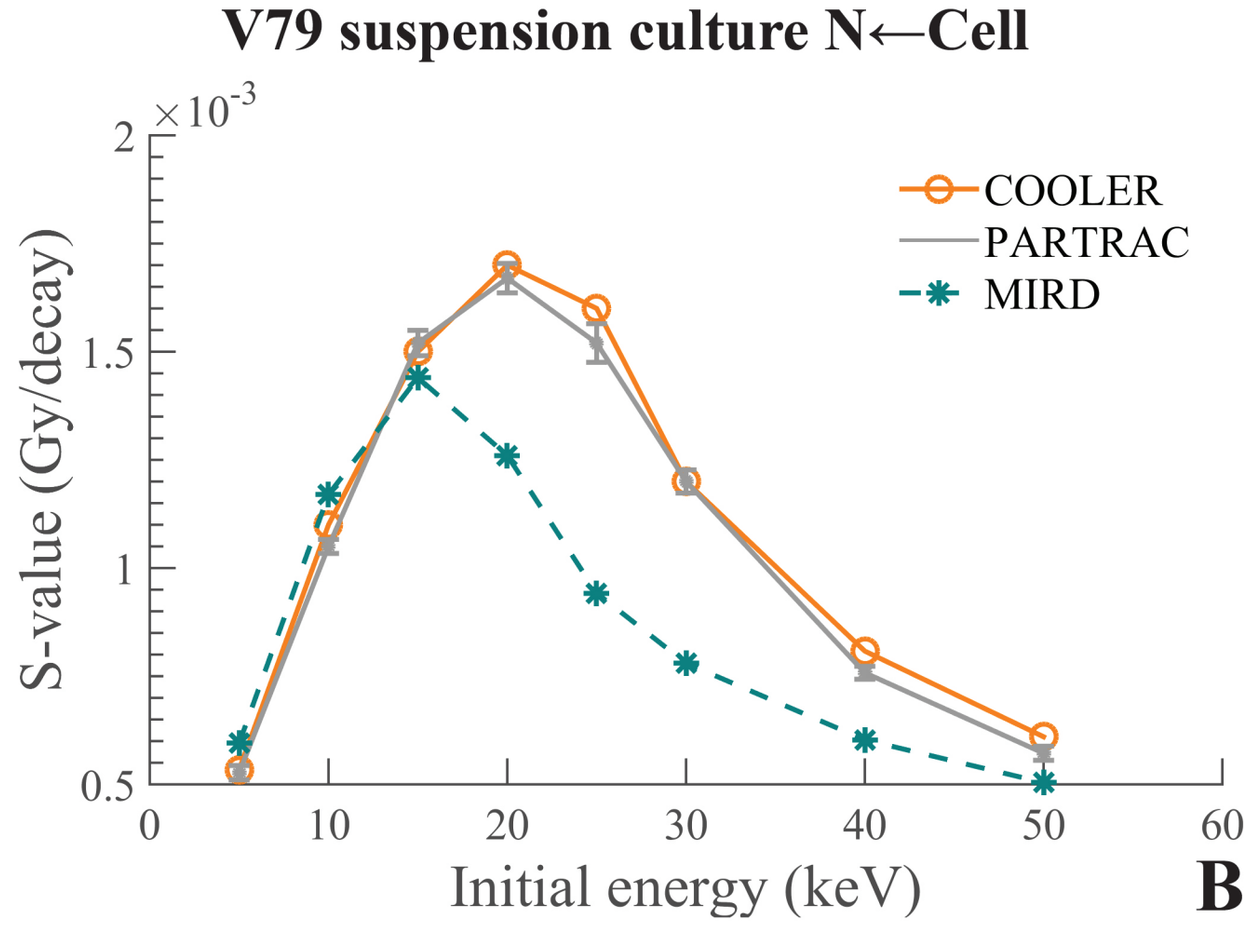
V79 suspension culture N←Cell
×10-3
S-value (Gy/decay)
Initial energy (keV)
COOLER
PARTRAC
MIRD
B

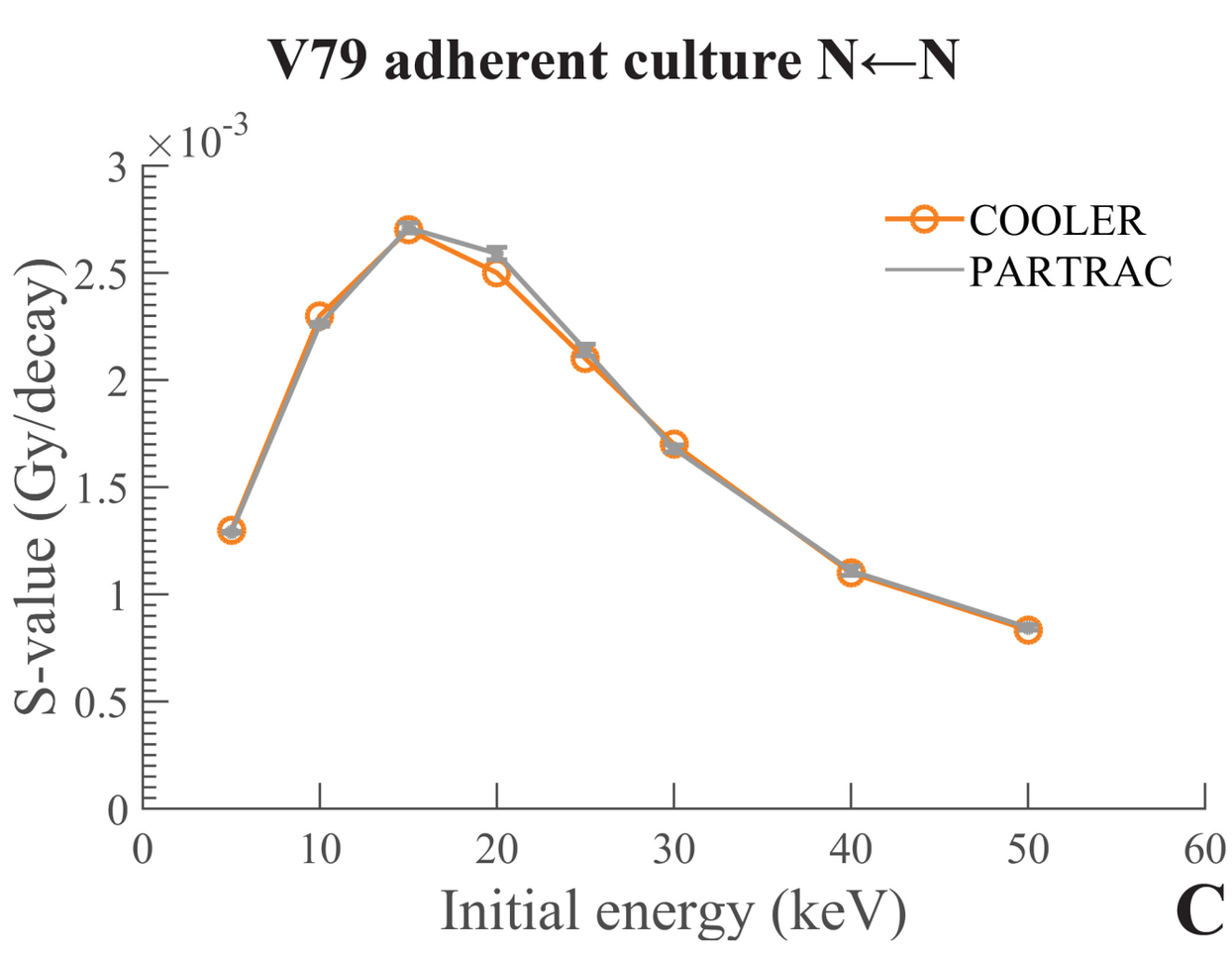
V79 adherent culture N←N
×10-3
S-value (Gy/decay)
Initial energy (keV)
COOLER
PARTRAC
C

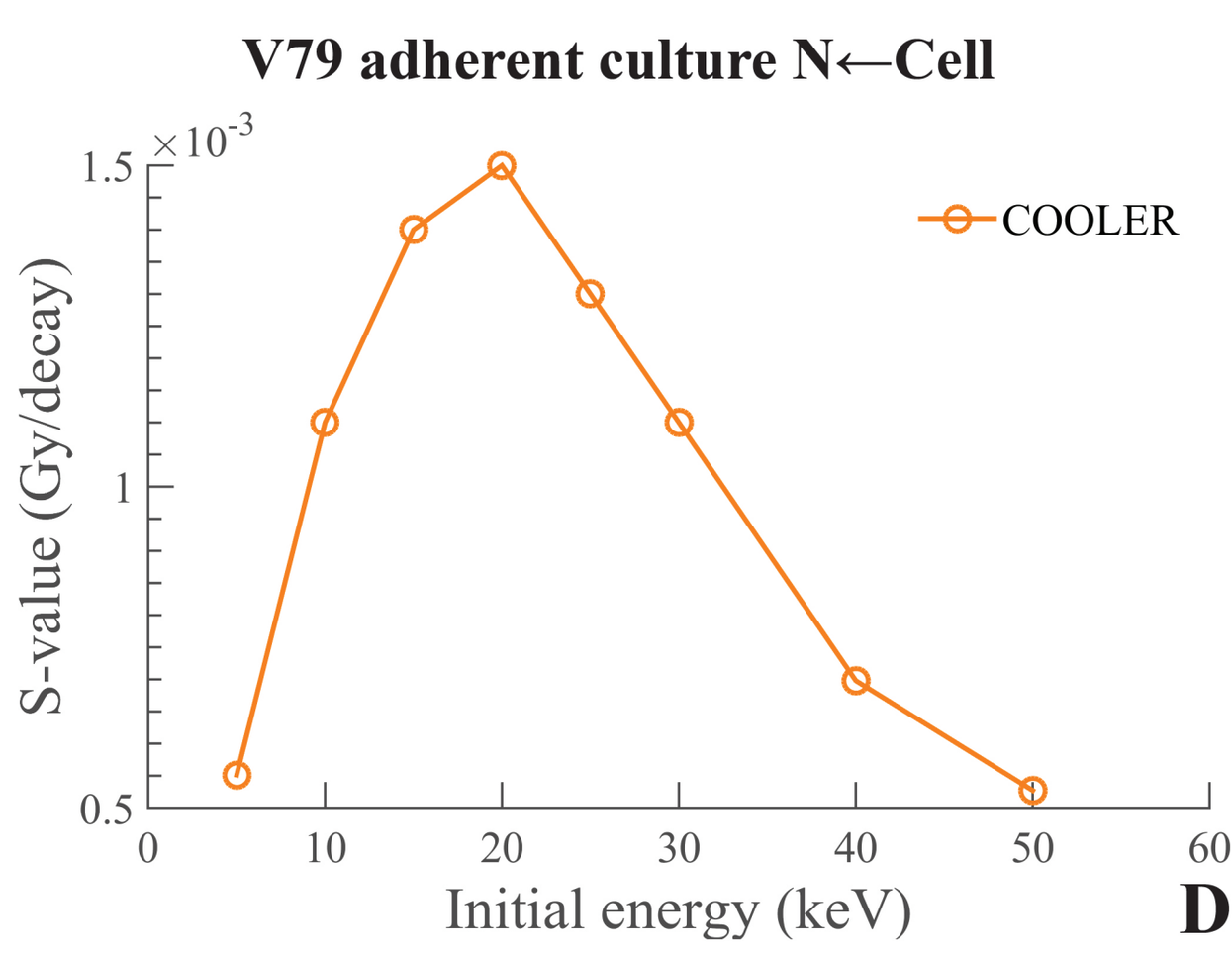
V79 adherent culture N←Cell
×10-3
S-value (Gy/decay)
Initial energy (keV)
COOLER
D

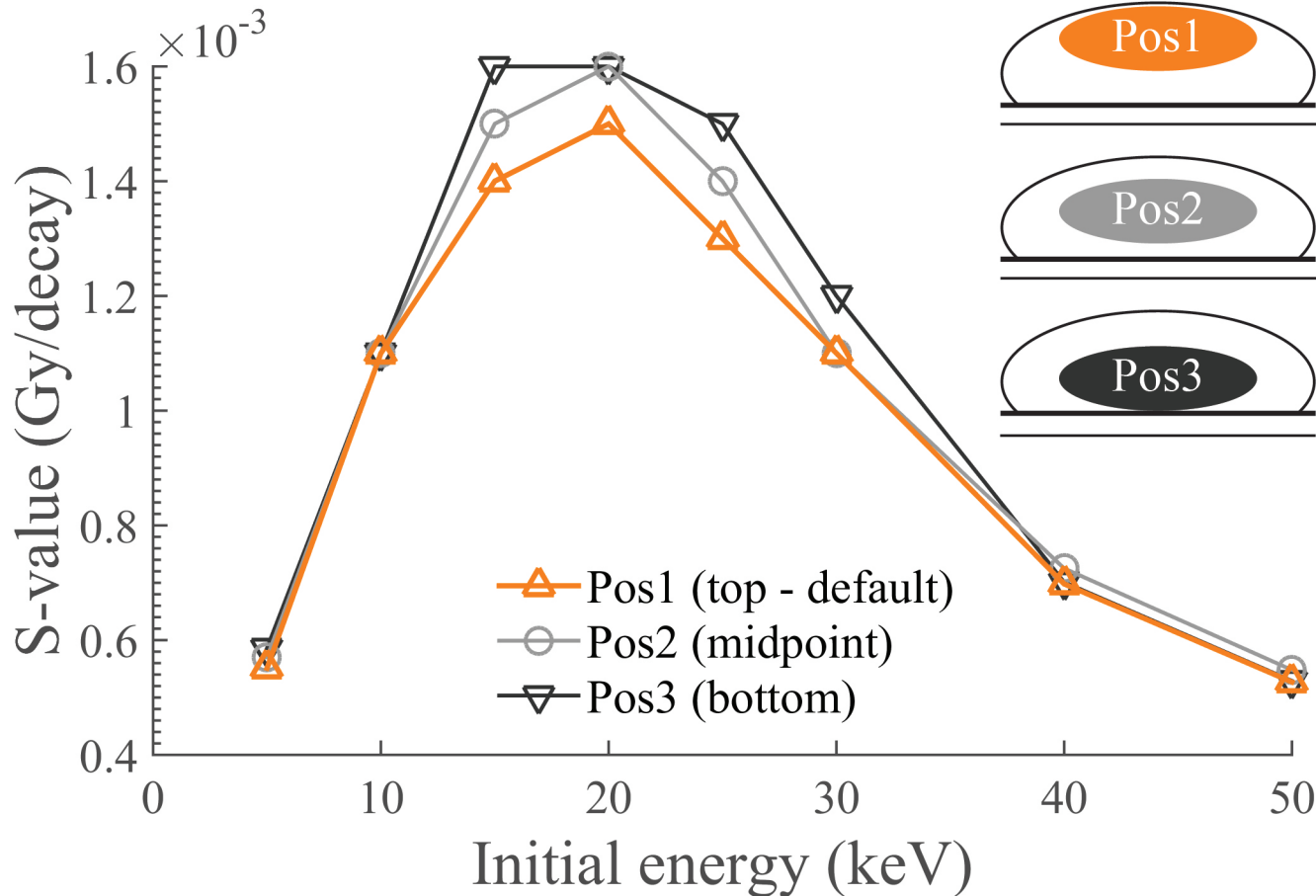
×10-3
1.6
1.4
1.2
1
0.8
0.6
0.4
S-value (Gy/decay)
0
10
20
30
40
50
Initial energy (keV)
Pos1 (top - default)
Pos2 (midpoint)
Pos3 (bottom)
Pos1
Pos2
Pos3